GEOPHYSICS, VOL. 75, NO. 6 (NOVEMBER-DECEMBER 2010); P. S249–S257, 9 FIGS., 4 TABLES.
10.1190/1.3517745

On the selection of reference velocities for split-step Fourier and generalized-screen migration methods

Jing-Bo Chen[1]

ABSTRACT

Split-step Fourier and generalized-screen migration methods are approximations with separation of variables to the one-way wave operator, in which the separation of space and wavenumber variables makes it possible to use the discrete fast Fourier transform to achieve computational efficiency. Both methods require the selection of reference velocities. Different choices of reference velocities lead to different velocity perturbations, and the smaller the velocity perturbations, the better the final image quality. The benefits of selecting a more representative reference velocity for the split-step Fourier method can be extended to the generalized-screen method by removing the limitation on the reference velocity for the generalized-screen method. Numerical experiments on the Marmousi model demonstrate the improvement of imaging by using an average velocity instead of the minimum velocity as the reference velocity for the generalized-screen method.

INTRODUCTION

Seismic migration is a wave-equation-based process that creates the image of structures within the earth from recorded data on the surface. With its scope increasingly broadening, seismic migration has now become a central step in seismic data processing (Gray et al., 2001). Seismic migration algorithms can be classified into two categories: integral methods and wavefield-continuation methods (Biondi, 2006).

Wavefield-continuation methods are more suited to image regions with complex geology. Split-step Fourier (SSF) and generalized-screen (GS) methods are wavefield-continuation methods (Stoffa et al., 1990; Le Rousseau and de Hoop, 2001). By introducing a reference velocity, these two methods can be formulated as separable approximations of the one-way wave operator (Chen and Liu 2004, 2006; Chen et al., 2007). Separable approximations of the one-way wave operator are also called approximations with separation of variables. The separation of space and wavenumber variables characterizes separable approximations and makes it possible to use the discrete fast Fourier transform to reduce computational cost. Approximations with separation of variables can also be applied to reverse-time migrations because the two-way wave equation can be cast into a wave equation in the form of the one-way wave operator by introducing a complex-valued wave equation (Zhang and Zhang, 2009).

The SSF method applies to media with weak lateral velocity variations. The GS method is a generalization of the SSF method and applies to media with strong lateral velocity variations at a higher computational cost in comparison with the SSF method. However, an advantage of the SSF method is not inherited in the GS method; that is, there is no limitation on reference velocities for the SSF method, whereas for the GS method, the reference velocity is required to be the minimum in the extrapolation interval to avoid singularity. Because no restriction is imposed on reference velocities for the SSF method, one can use an average velocity as the reference velocity that results in a small velocity perturbation. On the other hand, because of the minimum-velocity requirement of reference velocities for the GS method, the resulting velocity perturbation is relatively large, which compromises the higher accuracy of the GS method. Therefore, a problem occurs: How can one overcome the limitation on reference velocities for the GS method, thus take advantage of the smaller velocity perturbation, and so have higher fidelity in extrapolation? To give a solution to this problem, I carefully explore the mechanism of selecting a reference velocity for the SSF method and the associated influence of the reference velocity on the accuracy of the propagation. Based on this exploration, I show in this paper that the GS method can inherit the advantage of the SSF method in selecting a more representative reference velocity.

In the next section and Appendix A, I will present SSF and GS methods from a perspective of approximations with separation of variables. This is followed by an analysis on the influence of the reference velocity on the accuracy of the propagation for SSF and GS

Manuscript received by the Editor 24 January 2010; revised manuscript received 23 April 2010; published online 10 December 2010.
[1]Chinese Academy of Sciences, Institute of Geology and Geophysics, Key Laboratory of Petroleum Geophysics, Beijing, China. E-mail: chenjb@vip.sohu.com.

methods. I then perform some numerical experiments to demonstrate the theoretical analysis.

SSF AND GS METHODS

Consider the one-way wave operator in frequency-wavenumber domain

$$\mathcal{A}(x,y;k_x,k_y;\omega)=\exp\left\{\mathrm{i}\sqrt{\frac{\omega^2}{v(x,y)^2}-(k_x^2+k_y^2)}\Delta z\right\}, \tag{1}$$

where ω is circular frequency, k_x,k_y are wavenumbers, Δz is the continuation depth, and $v(x,y)$ is the velocity, which is averaged over z within a downward extrapolation interval.

The SSF method approximates the one-way wave operator (equation 1) as follows (Stoffa et al., 1990)

$$\mathcal{A}^{\mathrm{SSF}}=\exp\{\mathrm{i}k_z^{\mathrm{SSF}}\Delta z\}, \tag{2}$$

where v_r is the reference velocity, and k_z^{SSF} is the approximate vertical wavenumber

$$k_z^{\mathrm{SSF}}=\frac{\omega}{v}-\frac{\omega}{v_r}+\sqrt{\frac{\omega^2}{v_r^2}-(k_x^2+k_y^2)}. \tag{3}$$

The GS method approximates the one-way wave operator (equation 1) as follows (Le Rousseau and de Hoop, 2001)

$$\mathcal{A}^{\mathrm{GSn}}=\exp\{\mathrm{i}k_z^{\mathrm{GSn}}\Delta z\}, \tag{4}$$

where k_z^{GSn} is the approximate vertical wavenumber

$$k_z^{\mathrm{GSn}}=\frac{\omega}{v}-\frac{\omega}{v_r}+k_z^0+\omega\sum_{j=1}^{n}a_j\left(\frac{1}{v^2}-\frac{1}{v_r^2}\right)^j \times\left[\left(\frac{\omega}{k_z^0}\right)^{2j-1}-v_r^{2j-1}\right], \tag{5}$$

where $k_z^0=\sqrt{\frac{\omega^2}{v_r^2}-(k_x^2+k_y^2)}$, $a_1=\frac{1}{2}$, $a_j=(-1)^{j+1}\frac{1\cdot3\cdots(2j-3)}{j!2^j}$, $j\geq2$. SSF and GS methods belong to approximations with separation of variables of the one-way wave operator (equation 1). For details, see Appendix A.

SELECTION OF REFERENCE VELOCITIES

In this section, I discuss the issue of the selection of reference velocities for SSF and GS methods. First, the approximate vertical wavenumbers obtained by SSF and GS methods will be expressed in terms of propagation angles.

The approximate vertical wavenumber (equation 3) can be further written as

$$\begin{aligned}k_z^{\mathrm{SSF}}&=\frac{\omega}{v}-\frac{\omega}{v_r}+\sqrt{\frac{\omega^2}{v_r^2}-(k_x^2+k_y^2)}\\&=\frac{\omega}{v}\left\{1-\frac{v}{v_r}+\frac{v}{v_r}\sqrt{1-\frac{v_r^2}{v^2}\frac{v^2k_T^2}{\omega^2}}\right\}\\&=\frac{\omega}{v}\left\{1-\frac{v}{v_r}+\frac{v}{v_r}\sqrt{1-\frac{v_r^2}{v^2}\sin^2\alpha}\right\},\end{aligned} \tag{6}$$

where $k_T^2=k_x^2+k_y^2$ and α is the propagation angle.

Similarly, the approximate vertical wavenumber (equation 5) can be further formulated as

$$\begin{aligned}k_z^{\mathrm{GSn}}&=\frac{\omega}{v}-\frac{\omega}{v_r}+k_z^0+\omega\sum_{j=1}^{n}a_j\left(\frac{1}{v^2}-\frac{1}{v_r^2}\right)^j\left[\left(\frac{\omega}{k_z^0}\right)^{2j-1}-v_r^{2j-1}\right]\\&=\frac{\omega}{v}\left\{1-\frac{v}{v_r}+\frac{v}{v_r}\sqrt{1-\frac{v_r^2}{v^2}\frac{v^2k_T^2}{\omega^2}}+\frac{v}{v_r}\sum_{j=1}^{n}a_j\left(\frac{v_r^2}{v^2}-1\right)^jB_j\right\}\\&=\frac{\omega}{v}\left\{1-\frac{v}{v_r}+\frac{v}{v_r}\sqrt{1-\frac{v_r^2}{v^2}\sin^2\alpha}+\frac{v}{v_r}\sum_{j=1}^{n}a_j\left(\frac{v_r^2}{v^2}-1\right)^jB_j\right\},\end{aligned} \tag{7}$$

where $B_j=\left(\frac{1}{\sqrt{1-\frac{v_r^2}{v^2}\frac{v^2k_T^2}{\omega^2}}}\right)^{2j-1}-1=\left(\frac{1}{\sqrt{1-\frac{v_r^2}{v^2}\sin^2\alpha}}\right)^{2j-1}-1$. From equation 6, we can obtain the normalized vertical wavenumber for SSF:

$$\frac{v}{\omega}k_z^{\mathrm{SSF}}=1-\frac{v}{v_r}+\frac{v}{v_r}\sqrt{1-\frac{v_r^2}{v^2}\sin^2\alpha}. \tag{8}$$

From equation 7, we can obtain the normalized vertical wavenumber for GS:

$$\frac{v}{\omega}k_z^{\mathrm{GSn}}=1-\frac{v}{v_r}+\frac{v}{v_r}\sqrt{1-\frac{v_r^2}{v^2}\sin^2\alpha}+\frac{v}{v_r}\sum_{j=1}^{n}a_j\left(\frac{v_r^2}{v^2}-1\right)^jB_j. \tag{9}$$

In equation 8, when $v_r\leq v$, the normalized vertical wavenumber $vk_z^{\mathrm{SSF}}/\omega$ is real-valued for all propagation angles. On the other hand, when $v_r>v$, the normalized vertical wavenumber $vk_z^{\mathrm{SSF}}/\omega$ becomes complex-valued for propagation angles that are larger than $\alpha_{\max}=\sin^{-1}\left(\frac{v}{v_r}\right)$. We call $\alpha_{\max}$ the maximum propagation angle when the reference velocity v_r is larger than the true velocity v. In this case, wave propagation at angles beyond $\alpha_{\max}$ will become artificial evanescent waves and usually be discarded as follows (Han, 1998; Claerbout and Black, 2001)

$$\exp\left\{\mathrm{i}\sqrt{\frac{\omega^2}{v_r^2}-(k_x^2+k_y^2)}\Delta z\right\}=\begin{cases}\exp\left\{\mathrm{i}\sqrt{\frac{\omega^2}{v_r^2}-(k_x^2+k_y^2)}\Delta z\right\}, & k_x^2+k_y^2\leq\frac{\omega^2}{v_r^2},\\0, & k_x^2+k_y^2>\frac{\omega^2}{v_r^2}.\end{cases} \tag{10}$$

If we select a reference velocity that is the minimum velocity for the SSF method, the SSF method is valid for all propagation angles, but the velocity perturbation is large, which degrades the accuracy of the SSF method. On the other hand, if we choose an average velocity as the reference velocity for the SSF method, the resulting velocity perturbation decreases and the accuracy of the SSF method improves. Of course, there is a concern with the average reference velocity: Some velocities are larger than the reference velocity, but some velocities are smaller than the reference velocity, and in this case there is the issue of maximum propagation angles. In fact, there is no need to worry about this problem because for a given perturbation, the accuracy angle of the SSF method is smaller than the maximum propagation angle. See Tables 1 and 2 for details. The accuracy angle of the SSF method is defined as the angle at which the relative error between the normalized approximate vertical wavenumber and the exact one is less than or equal to 1%:

$$\left|\frac{vk_z^{\mathrm{SSF}}/\omega-\sqrt{1-\sin^2\alpha}}{\sqrt{1-\sin^2\alpha}}\right|\le 0.01. \tag{11}$$

Therefore, when artificial evanescent waves associated with propagation beyond the maximum angle are discarded, the accuracy of the SSF method is not affected.

Now we turn our attention to the GS method. In equation 9, when $v_r \le v$, the normalized vertical wavenumber $vk_z^{\mathrm{GSn}}/\omega$ is also real-valued for all propagation angles. When $v_r > v$, the normalized vertical wavenumber $vk_z^{\mathrm{GSn}}/\omega$ also becomes complex-valued for propagation angles beyond the maximum propagation angle and the artificial evanescent waves occur. The only difference between the SSF and GS method is that, at the maximum propagation angle $\alpha_{\max}$, the normalized vertical wavenumber $vk_z^{\mathrm{GSn}}/\omega$ becomes infinite (a singularity) whereas the normalized vertical wavenumber $vk_z^{\mathrm{SSF}}/\omega$ is still a finite real number. Therefore, if we discard the waves propagating at the maximum propagation angle and beyond as follows

$$\exp\left\{\mathrm{i}\sqrt{\frac{\omega^2}{v_r^2}-(k_x^2+k_y^2)}\Delta z\right\} = \begin{cases} \exp\left\{\mathrm{i}\sqrt{\frac{\omega^2}{v_r^2}-(k_x^2+k_y^2)}\Delta z\right\}, & k_x^2+k_y^2<\frac{\omega^2}{v_r^2}, \\ 0, & k_x^2+k_y^2\ge\frac{\omega^2}{v_r^2}, \end{cases} \tag{12}$$

we can remove the limitation on reference velocities for the GS method. Again, there is a concern with this removal: Will the issue of maximum propagation angles affect the accuracy of the GS method? The answer is no because just as with the SSF case, for a given velocity perturbation, the accuracy angle of the GS method is smaller than the maximum propagation angle (Tables 1 and 2). Therefore, we can use an average velocity as the reference velocity for the GS method to reduce the velocity perturbation, which can avoid the low accuracy caused by large velocity perturbations.

For completeness, the accuracy angles for SSF and GS methods for the case of $v_r \le v$ are also listed in Tables 3 and 4.

NUMERICAL EXPERIMENTS

In this section, numerical experiments will be performed to demonstrate the analysis of the previous section. For brevity, I only consider the first-order GS method in the following experiments. Higher-order GS methods can be discussed in the same way.

Setting $n = 1$ in equation 9, one obtains the normalized vertical wavenumber for GS1:

$$\frac{v}{\omega}k_z^{\mathrm{GS1}} = 1-\frac{v}{v_r}+\frac{v}{v_r}\sqrt{1-\frac{v_r^2}{v^2}\sin^2\alpha}+\frac{1}{2}\frac{v}{v_r}\left(\frac{v_r^2}{v^2}-1\right)B_1, \tag{13}$$

Table 1. Maximum propagation angles and accuracy angles of SSF and GS when $v_r > v$ in terms of $\frac{v_r - v}{v}$.

$\frac{v_r - v}{v}$	5%	10%	15%	20%	25%	30%	35%	40%
$\alpha_{\max} = \sin^{-1}\left(\frac{v}{v_r}\right)$	72°	65°	60°	56°	53°	50°	47°	45°
Accuracy angle of SSF	31°	23°	19°	17°	15°	14°	13°	12°
Accuracy angle of GS1	53°	40°	32°	26°	21°	18°	16°	14°
Accuracy angle of GS2	61°	49°	39°	32°	26°	22°	18°	15°
Accuracy angle of GS3	63°	52°	43°	36°	30°	24°	19°	16°
Accuracy angle of GS4	64°	53°	45°	38°	31°	26°	20°	16°

where $B_1 = 1/\sqrt{1 - \frac{v_r^2}{v^2}\sin^2\alpha} - 1$.

In Figure 1, I show the normalized vertical wavenumbers versus propagation angles for SSF and GS1 methods for $(v_r - v)/v = -10\%$ and $(v_r - v)/v = -10\%$, respectively. The exact normalized vertical wavenumber is also plotted for comparison. For $(v_r - v)/v = -10\%$, the curves for SSF and GS1 are above the exact curve, and the GS1 curve is closer to the exact curve than the SSF curve because GS1 is more accurate than SSF. For $(v_r - v)/v = 10\%$, the SSF curve is below the exact curve, whereas the GS1 curve is still above the exact curve. In this case, the maximum propagation angle is 65°. In the vicinity of the maximum propagation angle, the error in GS1 increases.

Figure 2 shows impulse responses for SSF and GS1 in a medium with $v = 3000$ m/s. The reference velocity is taken as $v_r = 2700$ m/s. The spacings are taken as $\Delta x = \Delta z = 15$ m, and the numbers of horizontal and vertical sampling are $nx = nz = 256$. A Ricker wavelet with peak frequency of 35 Hz is placed at (1905 m, 0 m). Both impulse responses are inside of the exact curve (red curve). As is expected, the GS1 response is closer to the exact curve than SSF.

Figures 3 and 4 show impulse responses for SSF and GS1 in the same medium as in Figure 2, but the reference velocities are taken as $v_r = 3150$ and 3300 m/s, respectively. Figure 3 is the result of SSF. Both responses are outside of the exact curve. With the reference ve-

Table 2. Maximum propagation angles and accuracy angles of SSF and GS when $v_r > v$ in terms of $\frac{v - v_r}{v_r}$.

$\frac{v - v_r}{v_r}$	−4.8%	−9.1%	−13.1%	−16.7%	−20%	−23.1%	−25.9%	−28.6%
$\alpha_{\max} = \sin^{-1}\left(\frac{v}{v_r}\right)$	72°	65°	60°	56°	53°	50°	47°	45°
Accuracy angle of SSF	31°	23°	19°	17°	15°	14°	13°	12°
Accuracy angle of GS1	53°	40°	32°	26°	21°	18°	16°	14°
Accuracy angle of GS2	61°	49°	39°	32°	26°	22°	18°	15°
Accuracy angle of GS3	63°	52°	43°	36°	30°	24°	19°	16°
Accuracy angle of GS4	64°	53°	45°	38°	31°	26°	20°	16°

Table 3. Accuracy angles of SSF and GS when $v_r \le v$ in terms of $\frac{v_r - v}{v}$.

$\frac{v_r - v}{v}$	−5%	−10%	−15%	−20%	−25%	−30%	−35%	−40%
Accuracy angle of SSF	31°	23°	19°	17°	15°	14°	13°	12°
Accuracy angle of GS1	57°	44°	35°	29°	24°	21°	19°	17°
Accuracy angle of GS2	68°	57°	48°	41°	34°	29°	25°	22°
Accuracy angle of GS3	73°	64°	57°	50°	43°	37°	31°	27°
Accuracy angle of GS4	75°	68°	62°	56°	50°	43°	37°	32°

Table 4. Accuracy angles of SSF and GS when $v_r \le v$ in terms of $\frac{v - v_r}{v_r}$.

$\frac{v - v_r}{v_r}$	5.3%	11.1%	17.6%	25%	33.3%	42.9%	53.8%	66.7%
Accuracy angle of SSF	31°	23°	19°	17°	15°	14°	13°	12°
Accuracy angle of GS1	57°	44°	35°	29°	24°	21°	19°	17°
Accuracy angle of GS2	68°	57°	48°	41°	34°	29°	25°	22°
Accuracy angle of GS3	73°	64°	57°	50°	43°	37°	31°	27°
Accuracy angle of GS4	75°	68°	62°	56°	50°	43°	37°	32°

locity increasing, the response is further away from the exact curve. Figure 4 is the result of GS1. In this case, the impulse responses are still inside of the exact curve, which is consistent with the result in Figure 2.

Now, I consider a laterally variant medium with velocity

$$v(x,z) = [2700 + 0.2(x - 1905)] \text{ m/s}. \quad (14)$$

The model size and sampling as well as the source are the same as the previous homogeneous medium. For this medium, the exact impulse response curve is a semicircle with a radius of 13,500 sin $h(0.2t)$ m, and the center of the semicircle is located at ({1905–13,500[1 − cos $h(0.2t)$]} m,0 m).

Figures 5 and 6 show impulse responses for SSF and GS1 with the minimum velocity as the reference velocity and the average velocity as the reference velocity, respectively. The results of average reference velocity are closer to the exact curves than that of minimum reference velocity.

Figure 7 shows the migration results on the Marmousi model (Versteeg and Grau, 1991) for SSF and GS1 with the minimum and average velocities as the reference velocities, respectively. The SSF result with the minimum reference velocity is very poor, whereas replacement of the minimum reference velocity by the average reference velocity greatly improves the imaging quality. The GS1 result with the minimum reference velocity is much better than the corresponding result for SSF with the minimum reference velocity; however, compared with the SSF result with the average reference velocity, the GS1 result with the minimum reference velocity has a better imaging quality in the shallow areas and a worse imaging quality in the deep areas. Again, by replacing the minimum reference velocity

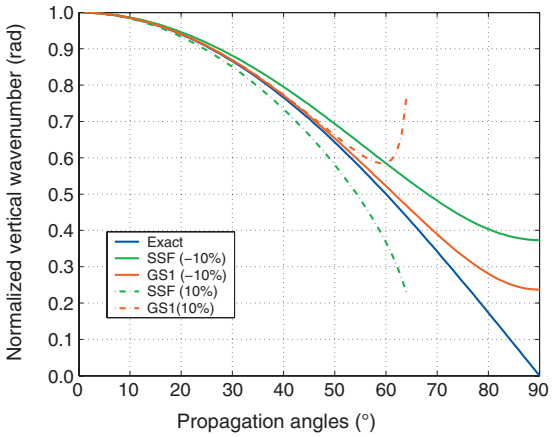

Figure 1. Normalized vertical wavenumbers versus propagation angles for SSF and GS1 methods for velocity errors $(v_r - v)/v = -10\%$ and $(v_r - v)/v = 10\%$, respectively.

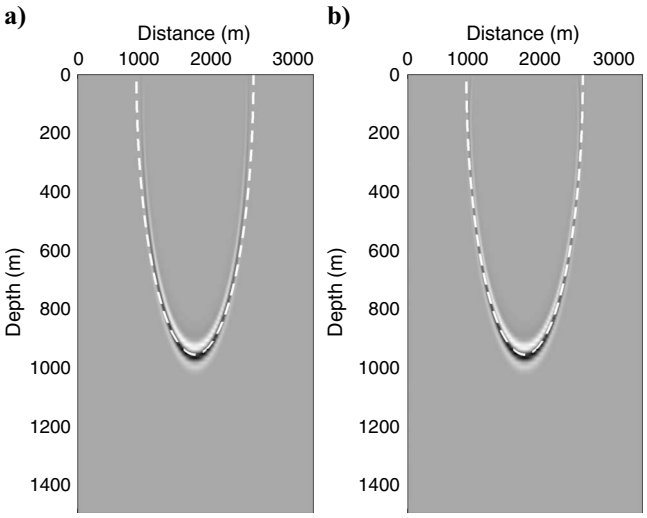

Figure 2. Impulse responses in a medium with $v = 3000$ m/s and $v_r = 2700$ m/s for (a) SSF and (b) GS1. The white dashed curve is the exact curve.

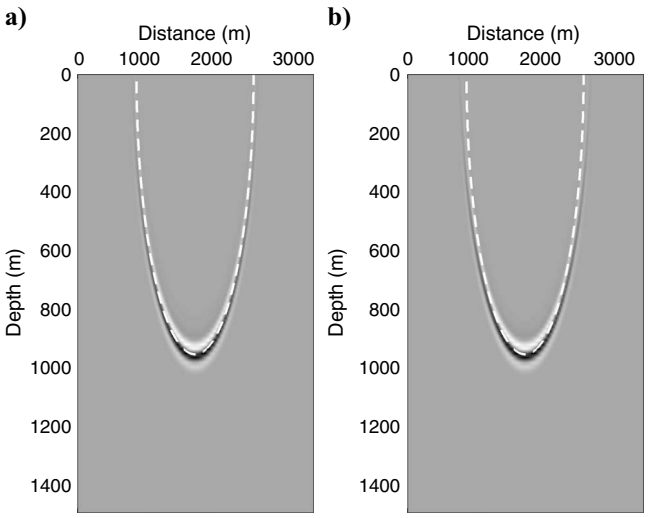

Figure 3. Impulse responses for SSF in a medium with $v = 3000$ m/s: (a) $v_r = 3150$ m/s and (b) $v_r = 3300$ m/s.

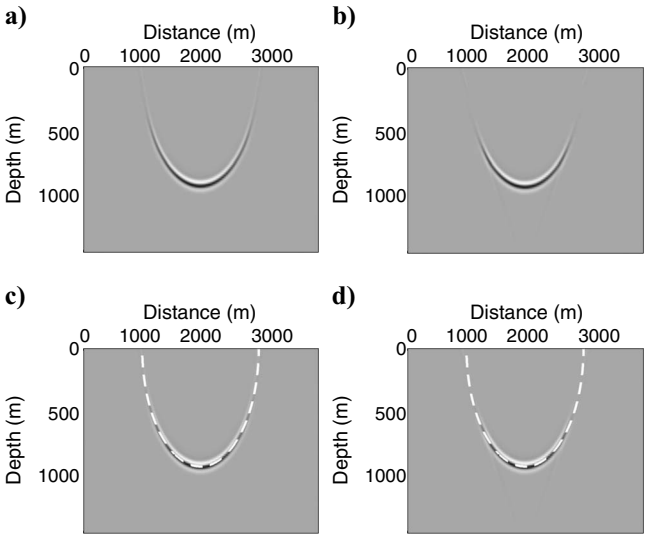

Figure 4. Impulse responses for GS1 in a medium with $v = 3000$ m/s: (a) $v_r = 3150$ m/s, (b) $v_r = 3300$ m/s, (c) plot a with the superimposed exact curve (white dashed curve), and (d) plot b with the superimposed exact curve (white dashed curve).

by the average reference velocity, the result of GS1 improves a lot, especially in the deep areas.

Three kinds of average velocities are available: arithmetic average, geometric average, and harmonic average. Specifically, suppose that there are n velocities at a certain depth level $v_i, i = 1,2,\ldots,n$, the three kinds of average velocities are

1. Arithmetic average: $v_a = \dfrac{v_1 + v_2 + \cdots + v_n}{n}$, (15)

2. Geometric average: $v_g = \sqrt[n]{v_1 v_2 \cdots v_n}$, and (16)

3. Harmonic average: $v_h = \dfrac{1}{s}$, where s

$$= \frac{\dfrac{1}{v_1} + \dfrac{1}{v_2} + \cdots + \dfrac{1}{v_n}}{n}. \quad (17)$$

The quantity s in equation 17 is called the average slowness. There exists a relation between these three average velocities

$$v_h \le v_g \le v_a. \quad (18)$$

The harmonic average is used in obtaining the results in Figure 7. Figure 8 shows the results of SSF with geometric average and arithmetic average, respectively. One can see that these three average velocities generate very similar results. Therefore, one can choose any of these three average velocities in practice.

In the above migrations with the Marmousi model, I use a migration aperture $[r_n - a, s_n + a]$, where r_n and s_n are horizontal coordinates of the receiver with maximum offset and the shot point for the nth shot data, respectively, and $a = 100 \times 12.5$ m $= 1250$ m. There are 240 shot data and $r_n = 425 + 25 \times (n - 1)$ (m), $s_n = 3000 + 25 \times (n - 1)$ (m), and $n = 1,2,\ldots,240$. The minimum velocity and average velocity are taken over $[r_n - a, s_n + a] \times [0$ m$,3000$ m$]$ for different depths 0 m $\le z \le 3000$ m. As in Han (1998), one can also choose minimum velocity and average velocity over $[r_n, s_n] \times [0$ m$,3000$ m$]$. Figure 9 shows the migration results obtained with GS1, where the reference velocities are the minimum velocity and average velocity taken over $[r_n, s_n] \times [0$ m$,3000$ m$]$. Compared with the corresponding results in Figure 7, the result with the minimum reference velocity improves and the result with the average reference velocity basically remains the same. The improvement is because the minimum velocity over $[r_n, s_n] \times [0$ m$,3000$ m$]$ is a kind of average velocity over $[r_n - a, s_n + a] \times [0$ m$,3000$ m$]$. To suppress wraparound from the computational boundary, a nonreflecting boundary condition is used (Cerjan et al., 1985).

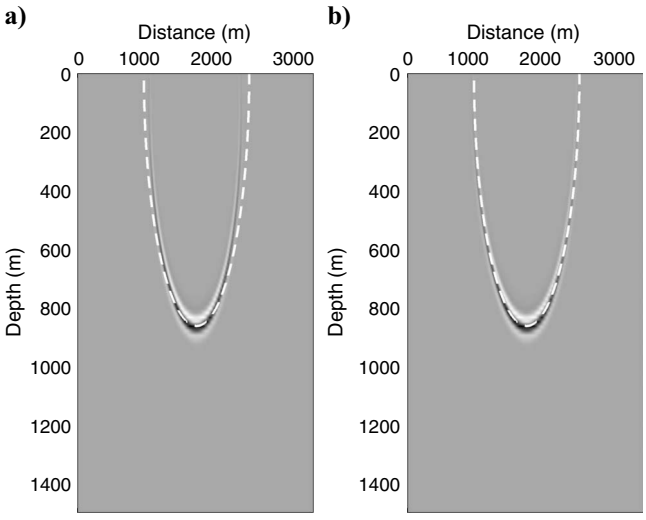

Figure 5. Impulse responses for SSF in a laterally variant medium: (a) with the minimum velocity as the reference velocity, and (b) with the average velocity as the reference velocity.

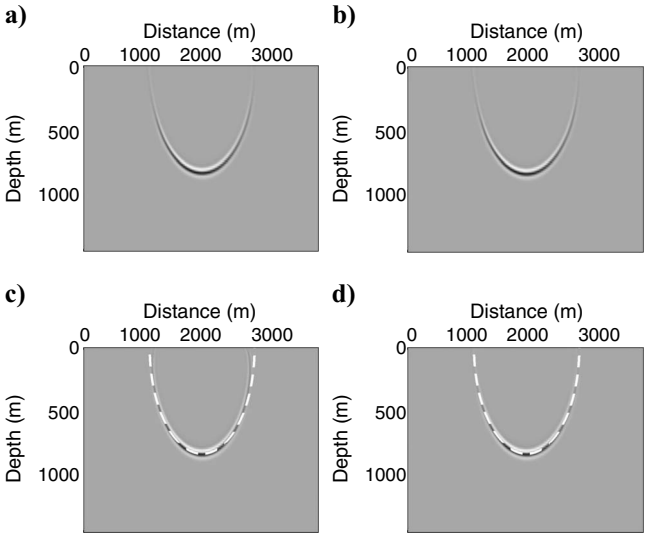

Figure 6. Impulse responses for GS1 in a laterally variant medium: (a) with the minimum velocity as the reference velocity, (b) with the average velocity as the reference velocity, (c) plot a with the superimposed exact curve (white dashed curve), and (d) plot b with the superimposed exact curve (white dashed curve).

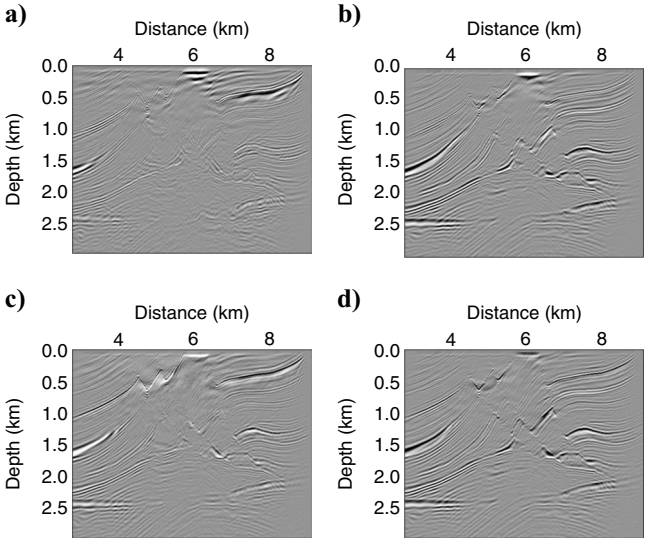

Figure 7. Migration results on Marmousi model. (a) SSF with the minimum velocity as the reference velocity. (b) SSF with the average velocity as the reference velocity. (c) GS1 with the minimum velocity as the reference velocity. (d) GS1 with the average velocity as the reference velocity.

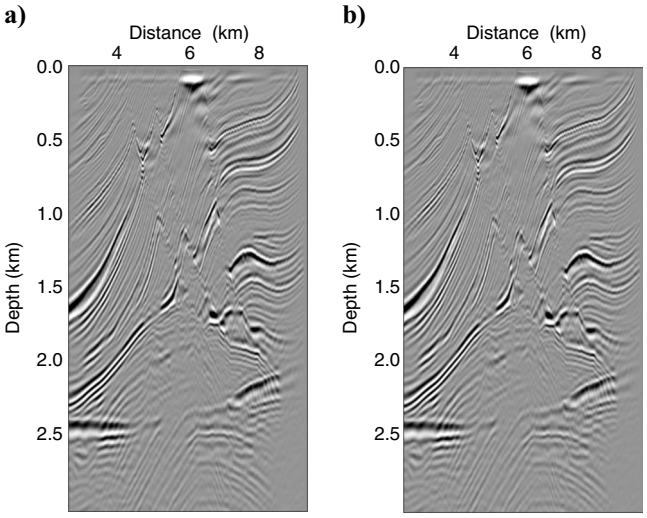

Figure 8. Migration results on the Marmousi model obtained with SSF: (a) with the arithmetic average as the reference velocity and (b) with the geometric average as the reference velocity.

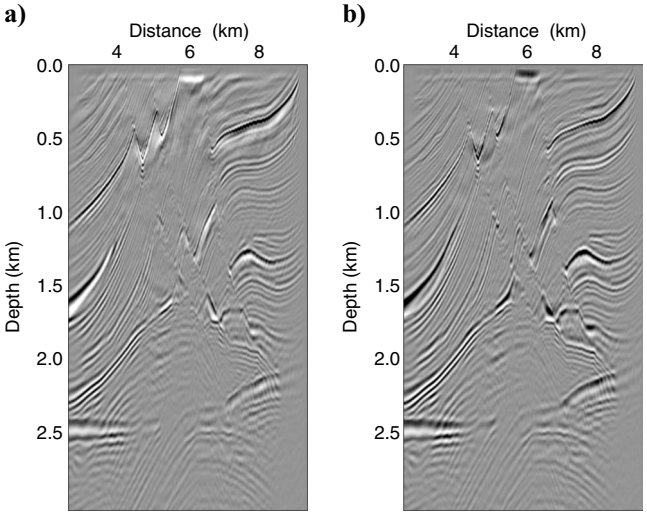

Figure 9. Migration results on the Marmousi model obtained with GS1: (a) the reference velocity is the minimum velocity taken over $[r_n,s_n]\times[0\text{ m},3000\text{ m}]$ and (b) the reference velocity is the average velocity taken over $[r_n,s_n]\times[0\text{ m},3000\text{ m}]$.

CONCLUSIONS

I have compared the selection of reference velocities for the SSF and GS methods. When the reference velocity is larger than the true velocity, both methods have the issue of the maximum propagation angle, and the maximum propagation angle is larger than the corresponding accuracy angle of the methods. Therefore, just like the SSF method, one can remove the limitation on the reference velocity of the GS method if one discards the artificial evanescent waves (the SSF case) plus the wave at the maximum propagation angle (singularity in the GS case) by setting them to be zero. With this removal, one can use an average velocity (arithmetic, geometric, or harmonic average) as the reference velocity to reduce velocity perturbations for achieving imaging improvement. Migration results on the Marmousi model demonstrate this imaging improvement.

ACKNOWLEDGMENTS

I thank the anonymous reviewers for valuable suggestions. This work is supported by National Natural Science Foundation of China under grants 40974074, 40774069, and 40830424.

APPENDIX A

SEPARABLE FORMULATIONS FOR THE SSF AND GS METHODS

The selection of a reference velocity leads to a separable formulation of the SSF and GS methods, which guarantees the applicability of FFT to improve computational efficiency. To gain a deep understanding for the separable properties of the SSF and GS methods, I present their separable formulations in this appendix.

Based on the one-way operator (equation 1), the wavefield-continuation formula can be written as

$$U(z+\Delta z,x,y;\omega)=\mathcal{F}^{-1}[\mathcal{A}(x,y;k_x,k_y;\omega)\mathcal{F}(U(z,x,y;\omega))], \tag{A-1}$$

where $U(z,x,y;\omega)$ is the wavefield at depth z, and $\mathcal{F}$ and $\mathcal{F}^{-1}$ denote the two-dimensional forward Fourier transform with respect to x and y and the inverse Fourier transform with respect to k_x and k_y, respectively.

The inverse Fourier transform in equation A-1 depends on the spatial variables x and y; therefore, we cannot directly apply FFT algorithms.

The separable approximation for the one-way operator (equation 1) is

$$\mathcal{A}(x,y;k_x,k_y;\omega)\approx\sum_{j=1}^{m}s_j(x,y;\omega)w_j(k_x,k_y;\omega), \tag{A-2}$$

where $s_j(x,y;\omega)$, and $w_j(k_x,k_y;\omega)$ $(j=1,2,\ldots,m)$ are called the separable base functions in spatial variables x and y and in wavenumber variables k_x and k_y, respectively, and m is referred to as the order of the separable approximation. The separable approximation is also called the approximation with separation of variables.

Using the separable approximation (equation A-2), equation A-1 becomes

$$U(z+\Delta z,x,y;\omega)=\sum_{j=1}^{m}\{s_j(x,y;\omega)\mathcal{F}^{-1}[w_j(k_x,k_y;\omega)\mathcal{F}(U(z,x,y;\omega))]\}. \tag{A-3}$$

Using equation A-3, FFT algorithms can be applied directly to achieve computational efficiency.

Based on equations 2 and 3, the separable approximation formula for SSF is

$$\mathcal{A}^{\mathrm{SSF}}(x,y;k_x,k_y;\omega) = s_1(x,y;\omega)w_1(k_x,k_y;\omega), \quad \text{(A-4)}$$

where

$$s_1(x,y;\omega) = \exp\left\{i\left(\frac{\omega}{v} - \frac{\omega}{v_r}\right)\Delta z\right\}$$

,

$$w_1(k_x,k_y;\omega) = \exp\left\{i\sqrt{\frac{\omega^2}{v_r^2} - (k_x^2 + k_y^2)}\Delta z\right\}$$

.

The construction of the GS algorithm consists of three steps: the approximation of the square root in equation 1, the approximation of the exponential in equation 1, and normalization of the resulting approximation (Le Rousseau and de Hoop, 2001). The first-step approximation of the one-way wave operator (equation 1) is equations 4 and 5.

The second step of constructing the GS algorithm approximates the exponential as

$$\mathcal{A}^{\mathrm{GSn}} = \exp\left\{\mathrm{i}\left[\frac{\omega}{v} - \frac{\omega}{v_r} + k_z^0 + R\right]\Delta z\right\} \times \approx \exp\left\{\mathrm{i}\left[\frac{\omega}{v} - \frac{\omega}{v_r} + k_z^0\right]\Delta z\right\}\{1 + \mathrm{i}R\Delta z\}, \quad \text{(A-5)}$$

where

$$R = \omega\Sigma_{j=1}^{n} a_j\left(\frac{1}{v^2} - \frac{1}{v_r^2}\right)^j\left[\left(\frac{\omega}{k_z^0}\right)^{2j-1} - v_r^{2j-1}\right]$$

.

Therefore, the separable approximation formula for the GS algorithm is

$$\mathcal{A}^{\mathrm{GSn}}(x,y;k_x,k_y;\omega) = \sum_{j=1}^{n+1} s_j(x,y;\omega)w_j(k_x,k_y;\omega), \quad \text{(A-6)}$$

where

$$s_1(x,y;\omega) = \exp\left\{i\left(\frac{\omega}{v} - \frac{\omega}{v_r}\right)\Delta z\right\},$$

$$w_1(k_x,k_y;\omega) = \exp\left\{i\sqrt{\frac{\omega^2}{v_r^2} - k_x^2 - k_y^2}\Delta z\right\},$$

$$s_{j+1}(x,y;\omega) = i\omega\Delta z a_j \exp\left\{i\left(\frac{\omega}{v} - \frac{\omega}{v_r}\right)\Delta z\right\}\left(\frac{1}{v^2} - \frac{1}{v_r^2}\right)^j,$$

$$w_{j+1}(k_x,k_y;\omega) = \exp\left\{i\sqrt{\frac{\omega^2}{v_r^2} - k_x^2 - k_y^2}\Delta z\right\} \times\left[\left(\sqrt{\frac{1}{v_r^2} - \frac{k_x^2}{\omega^2} - \frac{k_y^2}{\omega^2}}\right)^{-(2j-1)} - v_r^{2j-1}\right],$$

and

$$j = 1,2,\ldots,n.$$

Note that $s_1(x,y;\omega)$ and $w_1(x,y;\omega)$ in the separable approximation for the GS method are the same as that for the SSF method.

Finally, the third step for the GS algorithm is a normalization operation:

$$\mathcal{A}^{\mathrm{GSn}} = s_1(x,y;\omega)w_1(k_x,k_y;\omega)\mathcal{N} \times\left[1 + \frac{\sum_{j=2}^{n+1} s_j(x,y;\omega)w_j(k_x,k_y;\omega)}{s_1(x,y;\omega)w_1(k_x,k_y;\omega)}\right], \quad \text{(A-7)}$$

where $\mathcal{N}$ is a normalization operator defined as

$$\mathcal{N}(1+\alpha) = \exp(\mathrm{i}\Im(\alpha))\left|1 + \frac{\Re(\alpha)}{1 + \mathrm{i}\Im(\alpha)}\right|^{-1} \times\left[1 + \frac{\Re(\alpha)}{1 + \mathrm{i}\Im(\alpha)}\right], \quad \text{(A-8)}$$

where α is an arbitrary complex number, and $\Re(\alpha)$ and $\Im(\alpha)$ are its real and imaginary part, respectively (De Hoop et al., 2000).

The final nth-order GS algorithm (equation A-7) has two methods of implementation when applied to the initial wavefield $U(z,x,y;\omega)$:

$$U(z+\Delta z,x,y;\omega) = s_1(x,y;\omega)\mathcal{F}^{-1}[w_1(k_x,k_y;\omega)\mathcal{F}(U(z,x,y;\omega)\ ] \times\mathcal{N}\left[1 + \frac{\sum_{j=2}^{n+1} s_j(x,y)\mathcal{F}^{-1}[w_j(k_x,k_y;\omega)\mathcal{F}(U(z,x,y;\omega)\ ]}{s_1(x,y;\omega)\mathcal{F}^{-1}[w_1(k_x,k_y;\omega)\mathcal{F}(U(z,x,y;\omega)\ ]}\right], \quad \text{(A-9)}$$

and

$$U(z+\Delta z,x,y;\omega) = \mathcal{F}^{-1}\left\{w_1(k_x,k_y;\omega)\mathcal{F}[s_1(x,y;\omega)U(z,x,y;\omega)] \times\mathcal{N}\left[1 + \frac{\sum_{j=2}^{n+1} w_j(k_x,k_y;\omega)\mathcal{F}[s_j(x,y;\omega)U(z,x,y;\omega)]}{w_1(k_x,k_y;\omega)\mathcal{F}[s_1(x,y;\omega)U(z,x,y;\omega)]}\right]\right\}. \quad \text{(A-10)}$$

The two implementations (equations A-9 and A-10) have the same kinematic characteristics (Chen and Du, 2010). It is more convenient to use equation A-10 for normalization (Le Rousseau and de Hoop, 2001).

REFERENCES

Biondi, B. L., 2006, 3-D seismic imaging: SEG.

Cerjan, C., D. Kosloff, R. Kosloff, and M. Reshef, 1985, A nonreflecting boundary condition for discrete acoustic and elastic wave equations: Geophysics, **50**, 705–708, doi: 10.1190/1.1441945.

Chen, J.-B., and S.-Y. Du, 2010, Kinematic characteristics and the influence of reference velocities of phase-shift-plus-interpolation and extended-split-step-Fourier migration methods: Geophysical Prospecting, **58**, 429–439, doi: 10.1111/j.1365-2478.2009.00845.x.

Chen, J.-B., and H. Liu, 2004, Optimization approximation with separable variables for the one-way wave operator: Geophysical Research Letters, **31**, L06613, doi: 10.1029/2004GL019429.

Chen, J.-B., and H. Liu, 2006, Two kinds of separable approximations for the

one-way operator: Geophysics, **71**, no. 1, T1–T5, doi: 10.1190/1.2159059.
Chen, J.-B., H. Liu, and Z.-F. Zhang, 2007, A separable-kernel decomposition method for approximating the DSR continuation operator: Geophysics, **72**, no. 1, S25–S31, doi: 10.1190/1.2399368.
Claerbout, J. F., and J. L. Black, 2001, Basic earth imaging: Stanford University.
de Hoop, M. V., J. H. Le Rousseau, and R.-S. Wu, 2000, Generalization of the phase-screen approximation for the scattering of acoustic waves: Wave Motion, **31**, 43–70, doi: 10.1016/S0165-2125(99)00026-8.
Gray, S. H., J. Etgen, J. Dellinger, and D. Whitmore, 2001, Seismic migration problems and solutions: Geophysics, **66**, 1622–1640, doi: 10.1190/1.1487107.
Han, B. N., 1998, A program for 2-D prestack common-shot split-step Fourier migration: Center for Wave Phenomena/Seismic Un*x Free Software Package.
Le Rousseau, J. H., and M. V. de Hoop, 2001, Modeling and imaging with the scalar generalized-screen algorithms in isotropic media: Geophysics, **66**, 1551–1568, doi: 10.1190/1.1487101.
Stoffa, P. L., J. T. Fokkema, R. M. de Luna Freir, and W. P. Kessinger, 1990, Split-step Fourier migration: Geophysics, **55**, 410–421, doi: 10.1190/1.1442850.
Versteeg, R., and G. Grau, eds., 1991, The Marmousi experience: Proceedings of the 1990 EAEG Workshop, 52nd Annual International Meeting.
Zhang, Y., and G.-Q. Zhang, 2009, One-step extrapolation method for reverse time migration: Geophysics, **74**, no. 4, A29–A33, doi: 10.1190/1.3123476.